SIAM J. NUMER. ANAL.
Vol. 25, No. 5, October 1988

ANALYSIS OF THE SOR ITERATION FOR THE 9-POINT LAPLACIAN*

LOYCE M. ADAMS†, RANDALL J. LEVEQUE‡, AND DAVID M. YOUNG§

This paper is dedicated to Werner C. Rheinboldt.

Abstract. The SOR iteration for solving linear systems of equations depends upon an overrelaxation factor ω. A theory for determining ω was given by Young ("Iterative methods for solving partial differential equations of elliptic types," *Trans. Amer. Math. Soc.*, 76(1954), pp. 92–111) for consistently ordered matrices. Here we determine the optimal ω for the 9-point stencil for the model problem of Laplace's equation on a square. We consider several orderings of the equations, including the natural rowwise and multicolor orderings, all of which lead to nonconsistently ordered matrices, and find two equivalence classes of orderings with different convergence behavior and optimal ω's. We compare our results for the natural rowwise ordering to those of Garabedian ("Estimation of the relaxation factor for small mesh size," *Math. Comp.*, 10 (1956), pp. 183–185) and explain why both results are, in a sense, correct, even though they differ. We also analyze a pseudo-SOR method for the model problem and show that it is not as effective as the SOR methods. Finally, we compare the point SOR methods to known results for line SOR methods for this problem.

Key words. SOR, consistently ordered, multicolor ordering

AMS(MOS) subject classification. 65

1. Introduction. The SOR method (successive overrelaxation) is a standard iterative method for solving linear systems of equations, particularly large sparse systems arising from partial differential equations. Convergence of the method is greatly affected by the choice of overrelaxation parameter ω. A standard model problem for analyzing SOR is the system of equations arising from a finite difference discretization of Laplace's equation on a rectangle with zero boundary data. The solution of this problem is identically zero; hence, the iterates of SOR also represent the error at each step. The convergence properties of SOR for the model problem also apply to Poisson's equation with general Dirichlet boundary data, since the errors will still satisfy the homogeneous equation.

The 5-point approximation to the Laplacian is

$$\begin{aligned} u_{j-1,k}+u_{j+1,k}+u_{j,k-1}+u_{j,k+1}-4u_{jk}&=0, \qquad j,k=1,2,\cdots,N-1,\\ u_{jk}&=0, \quad j=0,N \quad \text{or } k=0,N, \end{aligned} \tag{1.1}$$

where u_{jk} approximates the solution $u(x_j, y_k)$ with $x_j = jh$, $y_k = kh$, and $h = 1/N$. This gives a linear system of $(N-1)^2$ equations in $(N-1)^2$ unknowns. The exact form of the matrix equation, and the form that the SOR iteration takes, depends on the order in which the unknowns u_{jk} are arranged in the vector of unknowns. Two standard

* Received by the editors October 28, 1986; accepted for publication (in revised form) July 14, 1987. This research was supported in part by NASA contract NAS1-18107 and AFOSR contract 85-0189 while the authors were in residence at the Institute for Computer Applications in Science and Engineering (ICASE) at NASA Langley Research Center.

† University of Washington, Seattle, Washington 98195. The research of this author was supported in part by U.S. Air Force Office of Scientific Research grant 86-0154.

‡ University of Washington, Seattle, Washington 98195. The research of this author was supported in part by National Science Foundation grant DMS-8601363.

§ University of Texas, Austin, Texas 78713. The research of this author was supported in part by Department of Energy grant DE-A505-81ER10954, National Science Foundation grant MCS-821473, and U.S. Air Force Office of Scientific Research grant 85-0052.

orderings are the natural rowwise (NR) ordering and the Red-Black (RB) ordering, in which the grid is colored in a checkerboard fashion and the Red points are ordered before the Black points (by rows within each color). For the model problem, the optimal ω and rate of convergence are the same for both of these orderings. This model problem was analyzed by Frankel [1950] and also by Young [1954], who gave a more general theory of SOR for a wide class of matrix equations in which the matrix is "consistently ordered."

Another standard model problem is the 9-point approximation to the Laplacian:

$$4u_{j-1,k}+4u_{j+1,k}+4u_{j,k-1}+4u_{j,k+1}+u_{j-1,k-1}+u_{j-1,k+1}+u_{j+1,k-1}+u_{j+1,k+1}-20u_{jk}=0,$$

$$j, k = 1, 2, \cdots, N-1, \tag{1.2}$$

$$u_{jk}=0, \quad j=0, N \quad \text{or } k=0, N.$$

Again there are various ways to order the unknowns, but none of these leads to a consistently ordered matrix and so the theory of Young does not apply. Multicolor orderings, similar to the RB ordering mentioned above but usually involving four colors for the 9-point stencil, are of particular interest for parallel processing applications. Recently Adams and Jordan [1986] have studied this problem in a more general context and identified 72 distinct four-color orderings. These can be grouped into equivalence classes that are known to have the same convergence behavior. For the model problem considered here, their theory reduces these to six classes of orderings that could potentially have different convergence rates, although the actual rate was not determined for any class.

In this paper, we analyze four of these six classes and show that these four classes can be reduced to two. One class is shown to have the same convergence behavior as the natural rowwise ordering, but the other class is shown to be distinct with a different optimal ω and asymptotic convergence rate. The eigenvectors of the iteration matrix are determined for three separate orderings and the corresponding eigenvalues (which determine the convergence rate) are found in terms of the roots of quartic equations. The optimal ω for small h is given by an asymptotic expansion about $h=0$, and is verified numerically.

In § 2 we use a separation of variables technique to determine the eigenvalues and eigenvectors for the NR ordering. The resulting quartic equation is used to derive the expansion for the optimal ω. Our results for this ordering differ from those given by Garabedian [1956]. We explain why both results are, in a sense, correct.

In § 3 we discuss the various multicolor orderings. The main technique we use is a change of variables from n, the iteration number, to ν, the "data flow time," as defined by Adams and Jordan [1986]. The fact that this change of variables can be used to simplify and relate various SOR methods was observed by LeVeque and Trefethen [1986]. They present a simple Fourier analysis of SOR on the 5-point stencil and show the equivalence of NR and RB using a change of variables motivated by Garabedian [1956] that is equivalent to the data flow times.

In § 4 we analyze a pseudo-SOR method based on a Red-Black coloring for the 9-point stencil. Although this method has attractive features for parallel computers, we show that it is unsatisfactory, being an order of magnitude slower than the true SOR methods with optimal ω.

Finally, in § 5, we briefly discuss line SOR methods and compare their convergence rates with the point SOR methods discussed in this paper. We summarize results for the 5-point and 9-point point and line SOR methods in Fig. 5.2.

2. Analysis of the natural rowwise ordering. For the 9-point stencil with NR ordering, the SOR method takes the form

$$u_{jk}^{n+1} = (1-\omega)u_{jk}^{n} + \frac{\omega}{5}(u_{j,k-1}^{n+1} + u_{j-1,k}^{n+1} + u_{j+1,k}^{n} + u_{j,k+1}^{n}) \tag{2.1}$$
$$\frac{\omega}{20}(u_{j-1,k+1}^{n} + u_{j-1,k-1}^{n+1} + u_{j+1,k+1}^{n} + u_{j+1,k-1}^{n+1}).$$

We assume that this iteration has a solution of the form

$$u_{jk}^{n} = \lambda^{n} w(x_j, y_k). \tag{2.2}$$

Then λ is an eigenvalue of the iteration matrix, and the vector with components $w(x_j, y_k)$, $j, k = 1, \cdots, N-1$ is the corresponding eigenvector. Putting (2.2) into (2.1), cancelling a common factor of λ^n, and dropping the subscripts on x and y gives

$$\begin{aligned} \lambda w(x,y) = {} & \lambda\omega(\tfrac{1}{5}w(x-h,y) + \tfrac{1}{20}w(x-h,y-h) + \tfrac{1}{5}w(x,y-h) + \tfrac{1}{20}w(x+h,y-h)) \\ & + \omega(\tfrac{1}{5}w(x+h,y) + \tfrac{1}{20}w(x-h,y+h) + \tfrac{1}{5}w(x,y+h) + \tfrac{1}{20}w(x+h,y+h)) \\ & + (1-\omega)w(x,y). \end{aligned} \tag{2.3}$$

The eigenfunction $w(x, y)$ must be zero on the boundary of the unit square in view of the given boundary conditions.

We use separation of variables and let $w(x, y) = X(x)Y(y)$. We also set $\alpha = \lambda^{1/2}$. Substituting this into (2.3) and dividing by $X(x)Y(y)$ gives

$$\begin{aligned} \frac{\alpha^2+\omega-1}{\omega} = {} & \frac{1}{5}\left(\frac{\alpha^2 Y(y-h) + Y(y+h)}{Y(y)}\right) + \frac{1}{20}\left(\frac{\alpha^2 Y(y-h) + Y(y+h)}{Y(y)}\right) \\ & \left(\frac{X(x-h)+X(x+h)}{X(x)}\right) + \frac{1}{5}\left(\frac{\alpha^2 X(x-h) + X(x+h)}{X(x)}\right). \end{aligned} \tag{2.4}$$

Now let

$$Y(y) = \alpha^{y/h} \sin \eta y \tag{2.5}$$

to get

$$\frac{\alpha^2+\omega-1}{\omega} = \frac{2\alpha}{5}\cos \eta h + \frac{X(x-h)}{X(x)}\Phi_1 + \frac{X(x+h)}{X(x)}\Phi_2 \tag{2.6}$$

where

$$\Phi_1 = \frac{1}{5}\alpha^2 + \frac{\alpha}{10}\cos \eta h, \qquad \Phi_2 = \frac{1}{5} + \frac{\alpha}{10}\cos \eta h. \tag{2.7}$$

We note that Φ_1 and Φ_2 are independent of x and y and let

$$X(x) = (\Phi_1/\Phi_2)^{x/2h} \sin \xi x. \tag{2.8}$$

Then

$$\frac{\Phi_1 X(x-h) + \Phi_2 X(x+h)}{X(x)} = 2\Phi_1^{1/2}\Phi_2^{1/2}\cos \xi h,$$

and using this in (2.6) gives

$$\frac{\alpha^2+\omega-1}{\omega} - \frac{2\alpha}{5}\cos \eta h = 2\Phi_1^{1/2}\Phi_2^{1/2}\cos \xi h. \tag{2.9}$$

Squaring (2.9), using (2.7), and rearranging terms gives a quartic equation for α:

$$\begin{aligned}(2.10)\qquad &\alpha^4-[\tfrac{4}{5}\omega\cos\eta h+\tfrac{2}{25}\omega^2\cos^2\xi h\cos\eta h]\alpha^3\\ &-[2(1-\omega)-\tfrac{4}{25}\omega^2\cos^2\eta h+\tfrac{1}{25}\omega^2\cos^2\xi h(\cos^2\eta h+4)]\alpha^2\\ &+[\tfrac{4}{5}\omega(1-\omega)\cos\eta h-\tfrac{2}{25}\omega^2\cos^2\xi h\cos\eta h]\alpha+(1-\omega)^2=0.\end{aligned}$$

An eigenmode of the iteration matrix has the form

$$\begin{aligned}(2.11)\qquad u_{jk}^n&=\lambda^n X(x_j)\,Y(y_k)\\ &=\alpha^{2n+k}[(\Phi_1/\Phi_2)^{1/2}]^j\sin\xi x_j\sin\eta y_k.\end{aligned}$$

In order for the boundary conditions to be satisfied, ξ and η must be integer multiples of π. The eigenvalue is $\lambda=\alpha^2$, where α is a root of (2.10). Note that we must choose the correct square root of Φ_1/Φ_2 in (2.11) (recall that we squared (2.9) to obtain (2.10), introducing additional solutions). The correct sign for $\Phi_1^{1/2}\Phi_2^{1/2}$ is determined by the requirement that (2.9) be satisfied, and this gives the correct sign for $\Phi_1^{1/2}/\Phi_2^{1/2}$ as well.

The frequencies ξ and η each range over the values $\pi, 2\pi, \cdots, (N-1)(\pi/2)$. This gives a set of $(N-1)^2/4$ pairs of frequencies. Corresponding to each pair (ξ, η) there are four roots of the quartic (2.10). In general these roots are distinct, and so we obtain $(N-1)^2$ eigenvalues and eigenvectors, the correct number. When the roots are not distinct, principal vectors will be obtained and the number of eigenvectors will be less than $(N-1)^2$. Recall that for the 5-point discretization, a principal vector is associated with the optimal ω, (see, e.g., Young [1971]). We make no attempt here to determine the principal vectors or the values of ω for which they occur. However, by continuity, we do obtain all of the eigenvalues.

The frequencies $((N-1)/2+1)\pi, \cdots, (N-1)\pi$, which one might expect to be included as well, give repeats of the eigenvectors already found. Replacing ξ by $N\pi-\xi$ leaves (2.10) unchanged while replacing η by $N\pi-\eta$ simply negates the coefficients of α and α^3. In either case the squares of the roots are unchanged. The eigenmodes (2.11) are also unchanged by these frequency reflections.

The convergence rate of the method (for fixed ω) is determined by the spectral radius of the iteration matrix, which is

$$\rho=\max_{\xi,\eta}|\lambda(\xi,\eta)|.$$

To determine the optimal ω, we need to minimize ρ over ω.

To help characterize the roots of (2.10), we first solved the quartic numerically for various values of the parameters. For example, the solid lines in Fig. 2.1 (the +'s will be explained later) show the magnitude of the four roots plotted as a function of ω when $\xi=\eta=\pi$ for $h=1/10, 1/100$, and $1/1000$. When ω is small there are four real roots. As ω increases, two of the roots become complex conjugates. The optimal ω occurs when these complex roots intersect the largest real root. As ω increases further, two more roots become complex conjugates and near $\omega=2$ there are two complex conjugate pairs. The same behavior was observed for smaller values of h using various values of ξ and η.

We now show that these observations are correct by determining the optimal ω and corresponding spectral radius for small h. We let ω have the form

$$(2.12)\qquad \omega=2-k_1h+O(h^2)$$

as $h\to 0$. At each value of h, ξ and η range over $\pi, 2\pi, \cdots, (N-1)\pi/2$ where $N=1/h$, and so $\cos\xi h$ and $\cos\eta h$ are selected from a set of points in $[0, 1]$ that becomes dense

as $h \to 0$. At each h, the optimal ω is the one that minimizes the maximum root of (2.10) over all allowable choices of ξ and η. We will simplify the problem by making the replacement

$$\cos \xi h \to p, \qquad \cos \eta h \leftarrow q$$

in (2.10), and proceed to determine the maximum root of the resulting quartic equation over all p and q in $[0, 1]$ for fixed k_1. We will find that the maximum root occurs when $p = q = 1$. We will show that this implies that the lowest frequencies $\xi = \eta = \pi$ determine the spectral radius of the iteration matrix as $h \to 0$. Making this replacement in (2.10) yields

$$\begin{aligned}(2.13)\qquad &\alpha^4 - [\tfrac{4}{5}\omega q + \tfrac{2}{25}\omega^2 p^2 q]\alpha^3 - [2(1-\omega) - \tfrac{4}{25}\omega^2 q^2 + \tfrac{1}{25}\omega^2 p^2 (q^2+4)]\alpha^2 \\ &+ [\tfrac{4}{5}\omega(1-\omega)q - \tfrac{2}{25}\omega^2 p^2 q]\alpha + (1-\omega)^2 = 0.\end{aligned}$$

We wish to analyze the behavior of the roots of this equation as $h \to 0$ with ω of the form (2.12) and p and q fixed. To determine the limiting behavior we set $h = 0$, $\omega = 2$ in (2.13) to obtain

$$(2.14)\qquad \alpha^4 - [\tfrac{8}{5}q + \tfrac{8}{25}qp^2]\alpha^3 + [2 + \tfrac{16}{25}q^2 - \tfrac{4}{25}p^2(q^2+4)]\alpha^2 - [\tfrac{8}{5}q + \tfrac{8}{25}qp^2]\alpha + 1 = 0.$$

In this limit all the roots of (2.14) lie on the unit circle since they must have modulus no greater than one and product equal to $(1-\omega)^2 = 1$. Setting $\alpha = e^{i\theta}$ and multiplying by $e^{-2i\theta}$ reduces (2.14) to a quadratic equation for $\cos\theta$

$$2\cos^2\theta - (\tfrac{8}{5}q + \tfrac{8}{25}qp^2)\cos\theta + \tfrac{8}{25}q^2 - \tfrac{2}{25}p^2(q^2+4) = 0.$$

This equation has roots

$$(2.15a)\qquad \cos\theta_1 = \frac{q}{4}\left(\frac{8}{5} + \frac{8}{25}p^2\right) - \frac{p}{5}\sqrt{\frac{13}{5}q^2 + \frac{4}{25}p^2q^2 + 4}$$

and

$$(2.15b)\qquad \cos\theta_2 = \frac{q}{4}\left(\frac{8}{5} + \frac{8}{25}p^2\right) + \frac{p}{5}\sqrt{\frac{13}{5}q^2 + \frac{4}{25}p^2q^2 + 4}.$$

The corresponding roots of (2.14) are $e^{\pm i\theta_1}$ and $e^{\pm i\theta_2}$. From (2.15a), $-1 < \cos\theta_1 < 1$ for all $p, q \in [0, 1]$, and hence (2.14) always has at least one pair of nonreal roots. The right-hand side of (2.15b) is a strictly increasing nonnegative function of p and q for $p, q \in [0, 1]$ and gives $\cos\theta_2 = 1$ only for $p = q = 1$. Thus for $p = q = 1$, there are two real roots at $\alpha = 1$, but for all other choices of p and q (2.14) has four nonreal roots.

We now wish to determine the behavior of the roots of (2.13) as $h \to 0$ with ω of the form (2.12) for some fixed k_1 (we will optimize over k_1 later). If $(p, q) \neq (1,1)$, then for sufficiently small h, the perturbed equation (2.10) also has four nonreal roots, by continuity. This might also be true for $p = q = 1$ and will be true for k_1 sufficiently small, as we will see. For larger k_1, two roots are real and this case will be discussed separately below.

We assume for now that (2.13) has two complex pairs of roots, expand them about the limiting values, and look for roots of the form

$$(2.16)\qquad e^{\pm i\theta_1}(1 - \beta_1 h) + O(h^2), \qquad e^{\pm i\theta_2}(1 - \beta_2 h) + O(h^2),$$

where β_1 and β_2 could be complex but will in fact be real. From (2.13), we see that the product of the roots is $(1-\omega)^2$. Using (2.12) and (2.16) and equating the $O(h)$ terms yields

$$(2.17)\qquad \beta_1 + \beta_2 = k_1.$$

Similarly, the sum of the roots must be $(4/5)\omega q+(2/25)\omega^2 p^2 q$ and again equating the $O(h)$ terms yields

$$\beta_1 \cos\theta_1+\beta_2\cos\theta_2 = k_1(\tfrac{2}{5}q+\tfrac{4}{25}qp^2). \tag{2.18}$$

If $p\neq 0$ then $\cos\theta_1\neq\cos\theta_2$ and we can solve (2.17) and (2.18) for β_1 and β_2. Doing this and using (2.15a) and (2.15b) we obtain

$$\beta_1=\left(\frac{1}{2}-\frac{pq}{5\sqrt{(13/5)q^2+(4/25)p^2q^2+4}}\right)k_1, \tag{2.19a}$$

and

$$\beta_2=\left(\frac{1}{2}+\frac{pq}{5\sqrt{(13/5)q^2+(4/25)p^2q^2+4}}\right)k_1. \tag{2.19b}$$

By continuity, these expressions are also valid in the case $p=0$.

Since p and q are nonnegative, $\beta_1\leqq\beta_2$ and the maximum root of the quartic (2.13) (for p, q, k_1 fixed, assuming all roots are nonreal) has magnitude $1-\beta_1 h+O(h^2)$ as $h\to 0$. Maximizing this value over p and q *in* $[0,1]$, we find that the maximum occurs for $p=q=1$ where

$$\beta_1=\tfrac{11}{26}k_1. \tag{2.20}$$

Moreover, if we replace p and q by $\cos\xi h$ and $\cos\eta h$ with ξ and η fixed as $h\to 0$ (low frequencies) we obtain $\beta_1=(11/26)k_1+O(h)$ from (2.19a) and consequently the value of β_1 in (2.20) is valid for the discrete problem as well.

We conclude that if we vary ω as in (2.12) when $h\to 0$, and if the resulting quartic (2.13) has nonreal roots then the spectral radius of the iteration matrix will be $1-\beta_1 h+O(h^2)$ with β_1 given by (2.20). But we must still consider the possibility that two of the roots of (2.13) are real. Recall that this can only occur when $p=q=1$ and that in this case the limiting quartic (2.14) has a double root at $\alpha=1$. Setting $p=q=1$ in (2.13) we find that $\alpha=1$ is in fact a root for all ω. Recall, however, that in practice $p=q=1$ cannot occur for $h>0$ and the maximum value that p and q can actually take is $\cos\pi h=1-\frac{1}{2}\pi^2h^2+O(h^4)$. Consequently, we must return to the original quartic (2.10), set

$$\cos\xi h=1-\tfrac{1}{2}\xi^2h^2+O(h^4),\qquad \cos\eta h=1-\tfrac{1}{2}\eta^2h^2+O(h^4),$$

and look for a real root of the form

$$\alpha=1-c_1h-c_2h^2+O(h^3). \tag{2.21}$$

We take terms out to the $O(h^2)$ term because now the $O(h)$ terms will cancel identically and we obtain an expression for c_1 only by equating the coefficients of h^2. Also, we must extend the expansion in (2.12) as

$$\omega=2-k_1h-k_2h^2+O(h^3)$$

although the coefficients c_2 and k_2 will drop out. Using these expansions in (2.10) and equating coefficients of h^2 gives

$$13c_1^2-15k_1c_1+9(\xi^2+\eta^2)=0.$$

So,

$$c_1=\tfrac{15}{26}k_1\pm\tfrac{1}{26}\sqrt{225k_1^2-468(\xi^2+\eta^2)}. \tag{2.22}$$

We see that for a given choice of ξ and η, (2.10) has real roots only if c_1 is real, that is, only for

$$k_1^2 \geqq \tfrac{468}{225}(\xi^2+\eta^2). \tag{2.23}$$

The largest real root is obtained by taking the minus sign in (2.22) and choosing $\xi=\eta=\pi$. This gives

$$c_1 = \tfrac{15}{26}k_1 - \tfrac{1}{26}\sqrt{225k_1^2-936\pi^2} \tag{2.24}$$

which is real for $k_1 > 2.04\pi$.

We must still determine the complex roots in the case where there are two real roots. Take these to be of the form $e^{\pm i\theta}(1-\beta h)+O(h^2)$. From (2.10), the product of all four roots must be $(1-\omega)^2$. Using this form of the complex roots and (2.21) with c_1 given by (2.22) for the two real roots, equating coefficients of h in the product yields

$$-2\beta - \tfrac{30}{26}k_1 = -2k_1.$$

So,

$$\beta = \tfrac{11}{26}k_1.$$

Note that this agrees with the value of β_1 found previously in (2.20) for the largest root in the case of four complex roots. This indicates that it is the pair of complex roots with smaller magnitude that splits into real roots as the critical value of k_1 given by (2.23) is passed. This agrees with what is observed in Fig. 2.1.

We now determine the optimal ω. We need only minimize

$$\max(1-\beta_1 h, 1-c_1 h)$$

where β_1 and c_1 are given by (2.20) and (2.24), respectively. Since β_1 is an increasing function of k_1 and c_1 is decreasing function of k_1, the minimum occurs where $\beta_1 = c_1$ which gives

$$k_1 = \pi\sqrt{\tfrac{936}{209}} \approx 2.116\pi.$$

Consequently,

$$c_1 = \beta_1 = \tfrac{11}{26}k_1 \approx 0.895\pi$$

and the optimal ω and corresponding spectral radius, $\rho = \alpha^2 \approx 1-2c_1h$, have the values

$$\omega_{\text{opt}} = 2-2.116\pi h + O(h^2), \qquad \rho_{\text{opt}} = 1-1.791\pi h + O(h^2) \tag{2.25}$$

as $h \to 0$.

For comparison, the corresponding values for the 5-point model problem are

$$\omega_{\text{opt}}^{\text{5-pt}} \approx 2-2\pi h, \qquad \rho_{\text{opt}}^{\text{5-pt}} \approx 1-2\pi h.$$

Notice that for the 9-point stencil, the spectral radius is slightly larger, giving somewhat slower convergence than for the 5-point stencil, although the two are very close. More important, both are $1-O(h)$ as $h \to 0$, giving asymptotically the same order of convergence. By contrast the Jacobi and Gauss-Seidel methods, and also the pseudo-SOR method analyzed in § 4, have spectral radii $1-O(h^2)$ as $h \to 0$.

It is very interesting to compare these results with asymptotic results obtained by Garabedian [1956], especially since they do not agree and yet both are, in a sense, correct. Garabedian's analysis is based on viewing the SOR iteration (2.1) as a finite difference method for a time-dependent PDE. Expanding in Taylor series shows that this difference equation is consistent with the PDE

$$5Cu_t + 2u_{xt} + 3u_{yt} = 3u_{xx} + 3u_{yy}, \qquad u = 0 \text{ on the boundary} \tag{2.26}$$

where C and ω are related by

$$\omega = \frac{2}{1+Ch}. \tag{2.27}$$

If we fix $C>0$ and choose ω according to (2.27) for each $h>0$, then $0<\omega<2$, and so the method (2.1) is stable. Since it is consistent with the linear equation (2.26), iterates u_{jk}^n with $n=T/h$ must converge to solutions $u(x_j, y_k, T)$ of (2.26) as $h\to 0$ (by the Lax Equivalence Theorem) if we choose u_{jk}^0 by discretizing fixed initial data $u(x, y, 0)$. Consequently, studying the decay of solutions to (2.26) gives information about the rate of convergence of SOR.

By introducing the change of variables

$$s = t + \frac{x}{3} + \frac{y}{2},$$

(2.26) is transformed to

$$5Cu_s + \tfrac{13}{12}u_{ss} = 3u_{xx} + 3u_{yy}.$$

Separation of variables shows that eigenmodes of this PDE have the form

$$u(x, y, s) = e^{-ps} \sin \xi x \sin \eta y,$$

where ξ and η are integer multiples of π and $p = p(\xi, \eta)$ is a root of the quadratic equation

$$\tfrac{13}{12}p^2 - 5Cp + 3(\xi^2+\eta^2) = 0. \tag{2.28}$$

Transforming back to the original time variable gives

$$u(x, y, t) = e^{-p(t+x/3+y/2)} \sin \xi x \sin \eta y. \tag{2.29}$$

Note that in a time step of length h, this solution decays by a factor $e^{-\mathrm{Re}(p)h}$. The eigenmode with slowest decay is obtained by taking $\xi = \eta = \pi$ and the negative square root in solving (2.28), giving

$$p_{\min} = \tfrac{6}{13}(5C - \sqrt{25C^2 - 26\pi^2}). \tag{2.30}$$

If we obtain initial data for SOR by discretizing the corresponding eigenfunction, $u_{jk}^0 = u(x_j, y_k, 0)$ from (2.29), it follows (by convergence) that the decay factor for the SOR iteration must have the form

$$|\lambda_{\max}| = 1 - \mathrm{Re}\,(p_{\min})h + O(h^2) \tag{2.31}$$

as $h\to 0$. Since taking other eigenfunctions as initial data gives faster decay, one is led to the conclusion that in order to obtain the fastest possible convergence, we should maximize $\mathrm{Re}\,(p_{\min})$ and hence minimize $|\lambda_{\max}|$. Recall that the value of C is still at our disposal. We can minimize $\mathrm{Re}\,(p_{\min})$ by setting the radical to zero in (2.30), giving

$$C = \frac{\sqrt{26}}{5}\pi \approx 1.02\pi, \qquad p_{\min} = 6\pi\sqrt{2/13} \approx 2.35\pi.$$

By (2.27) and (2.31), we obtain the following predictions for the optimal ω and the corresponding decay rate, as in Garabedian [1956]:

$$\begin{aligned} \omega_{\mathrm{opt}}^* &= \frac{2}{1+Ch} \approx 2(1-Ch) = 2 - 2.04\pi h, \\ \rho_{\mathrm{opt}}^* &= e^{-p_{\min}h} \approx 1 - \rho_{\min}h = 1 - 2.35\pi h. \end{aligned} \tag{2.32}$$

These values do not agree with the values (2.25) found by computing the eigenvalues of the iteration matrix. The reason is the following. While (2.31) does indeed give a correct expression for the largest eigenvalue of the iteration matrix corresponding to a decay factor for the PDE, there are other, spurious, eigenvalues of the discrete problem that have larger magnitude for ω near 2 and hence determine the spectral radius ρ. This is seen clearly in Fig. 2.1, where we have plotted $|e^{-ph}|$ for the two roots of the quadratic (2.28) (as +'s) along with $|\lambda|$, the magnitudes of the actual eigenvalues obtained by solving the quartic (2.10) (as the solid lines). One pair of discrete eigenvalues closely matches $|e^{-ph}|$ for small h, while the other (complex conjugate) pair does not. In fact, Garabedian's results may also be obtained from our approach by choosing k_1 in (2.24) to maximize c_1, thereby ignoring the effect of the other root.

For each fixed h, we can choose initial data (namely, as a spurious eigenvector) so that convergence is slow and determined by the spectral radius. On the other hand, these spurious eigenvectors become highly oscillatory and do not approach a limit as $h \to 0$. In particular, they do not approach the eigenmodes of the PDE as $h \to 0$. Consequently, if we obtain our initial data by discretizing a fixed function of x and y at each h (as is more realistic in practice), we would expect to see vanishingly small components of these spurious eigenvectors as $h \to 0$. For practical purposes, then, the values (2.32) obtained by Garabedian may be more meaningful and useful than the "true" values (2.25).

This is demonstrated in Fig. 2.2, where we show the decay of $\|u\|_2$ for various initial data. For initial data obtained by discretizing the smooth data $u(x, y) = (x^2 - x)(y^2 - y)$, the observed decay is initially much closer to $|\lambda_{\max}|^n$, as predicted by (2.31), than to ρ^n. However, as the iteration continues we would expect to see the effect of the spurious eigenvectors take over. With the NR ordering on smooth initial data, this has not yet appeared over the number of iterations used. With different initial data, $u_{ij} = 1$ at all interior points (so that there is a discontinuity at the boundary where $u = 0$, and hence more high frequencies are present), this divergence does occur and the asymptotic slope appears to agree with the spectral radius. This effect is even more visible in Fig. 3.11 where the same experiments are performed for a different ordering. In that case, even with smooth initial data, the asymptotic convergence rate is clearly given by the spectral radius although down to an error level of 10^{-6} or so Garabedian's estimate is valid.

To verify that the eigenvector corresponding to the spectral radius is highly oscillatory, we note that by (2.5) and (2.8) an eigenvector has the form

$$w_{jk} = \alpha^k [(\Phi_1/\Phi_2)^{1/2}]^j \sin \xi x_j \sin \eta y_k. \tag{2.33}$$

Inserting a complex eigenvalue $\alpha = e^{i\theta}(1 - \beta h) + O(h^2)$ into (2.33) gives

$$w_{jk} = e^{i\theta k}(1 - \beta h)^k [(\Phi_1/\Phi_2)^{1/2}]^j \sin \xi x_j \sin \eta y_k.$$

Since $\theta \neq 0$, this function will be oscillatory in k and j and nonconvergent as $h \to 0$. By contrast, the eigenvector corresponding to the other pair of roots converges to the eigenfunctions (2.29) of the PDE as $h \to 0$. For these vectors our previous arguments show that λ has the form of (2.31) and hence α, the square root of λ, can be expressed as

$$\alpha = 1 - \tfrac{1}{2}ph + O(h^2). \tag{2.34}$$

Expanding Φ_1/Φ_2 using this value of α in (2.7) shows that

$$\Phi_1/\Phi_2 = 1 - \tfrac{2}{3}ph + O(h^2). \tag{2.35}$$

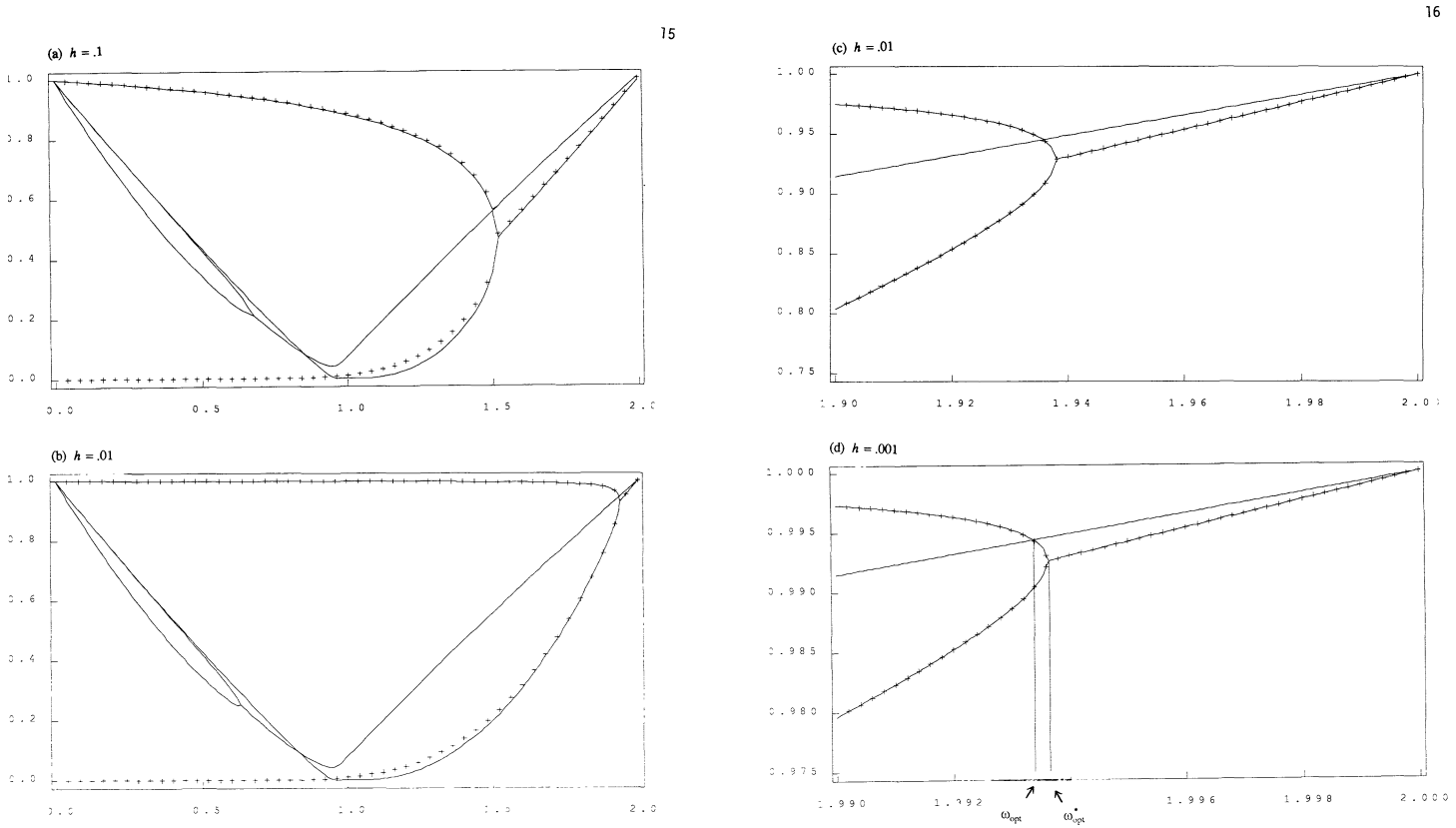

FIG. 2.1. *Solid lines show* $|\alpha^2| = |\lambda|$ *for the iteration matrix with* $\xi = \eta = \pi$, *obtained by solving the quartic* (2.10). *The symbols* + *show* e^{-ph} *where* p *is a root of the quadratic equation* (2.27) *with* $\xi = \eta = \pi$. (a) $h = .1$ *for* $0 \leqq \omega \leqq 2$. (b) $h = .01$ *for* $0 \leqq \omega \leqq 2$. (c) $h = .01$ *for* $1.9 \leqq \omega \leqq 2$. (d) $h = .001$ *for* $1.99 \leqq \omega \leqq 2$.

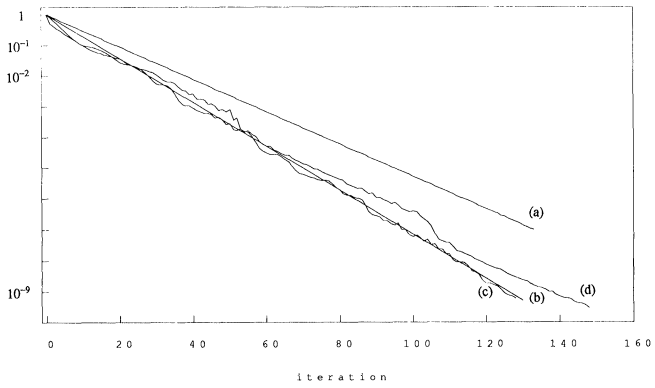

FIG. 2.2. *Convergence history (2-norm of error versus iteration number) for the* NR *ordering with* $h = 0.05$ *and* $\omega = 1.86$. *Three choices of initial data are compared*: (a) *An eigenvector corresponding to the spectral radius.* (b) *An eigenvector corresponding to the largest nonspurious eigenvalue.* (c) $u^0_{jk} = (x_j^2 - x_j)(y_k^2 - y_k)$. (d) $u^0_{jk} = 1$.

Putting (2.34) and (2.35) into (2.11) gives

$$u^n_{jk} = (1 - \tfrac{1}{2}ph + O(h^2))^{2n+k}(1 - \tfrac{1}{3}ph + O(h^2))^j \sin \xi jh \sin \eta kh$$
$$= (1 - ph + O(h^2))^{n+j/3+k/2} \sin \xi jh \sin \eta kh.$$

As $h \to 0$ with $t = nh$, $x = jh$ and $y = kh$ fixed, this approaches the eigenmode (2.29) of the PDE.

(See note added in proof.)

3. Multicolor SOR. In this section we consider the SOR method applied to the 9-point model problem with several alternative orderings of the unknowns u_{jk}. These orderings are determined by labeling the grid points with four different colors (Red, Black, Green, and Orange) and then ordering the points by first listing all the points of one color, then a second color, and so on. The overall ordering of grid points is determined by two factors: (a) the manner in which the grid points are labeled (the coloring of the grid) and (b) the order in which the colors are taken (the ordering of the colors).

Four-colorings are of interest for the 9-point stencil because with four colors it is possible to decouple the grid, in the sense that the resulting SOR formula for updating a grid point of any given color involves neighboring grid points, all of which have different colors than the center point. This is advantageous in parallel processing applications since all grid points of the same color can be updated simultaneously.

For the 5-point stencil, two colors suffice to decouple the grid using the RB checkerboard pattern discussed in § 1. Recently LeVeque and Trefethen [1986] have presented an easy way to analyze the 5-point model problem using a change of variables from the iteration number, n, to the earliest time, ν, that the unknown at a grid point can be updated assuming one update requires one time unit. This variable ν corresponds to the "data flow times" discussed in Adams and Jordan [1986] and closely resembles the change of variables used by Garabedian [1956] to analyze the PDE. This change of variables allows the use of Fourier analysis to determine the convergence rate and optimal ω. It also gives a straightforward proof of the equivalence of the NR and RB orderings.

Here we use this same approach to analyze the four-color orderings for the 9-point stencil. Before introducing these orderings, we briefly review the analysis for the 5-point NR and RB orderings to introduce notation and motivate our 9-point analysis.

For the 5-point model problem (1.1) with the NR ordering, the SOR iteration takes the form

$$u_{jk}^{n+1} = (1-\omega)u_{jk}^{n} + \frac{\omega}{4}(u_{j-1,k}^{n+1} + u_{j,k-1}^{n+1} + u_{j,k+1}^{n} + u_{j+1,k}^{n}). \tag{3.1}$$

The stencil for updating a grid point on iteration $n+1$ using the NR ordering is given in Fig. 3.1. To assist in determining the change of variables, the earliest times at which an unknown can be updated on the first two iterations using the stencil in Fig. 3.1 are listed below each node in Fig. 3.2. These times define the iteration variable ν. Each node in Fig. 3.2 is updated at time $\nu+1$ by the stencil shown in Fig. 3.3, and the corresponding SOR iteration is

$$u_{jk}^{\nu+1} = (1-\omega)u_{jk}^{\nu-1} + \frac{\omega}{4}(u_{j-1,k}^{\nu} + u_{j,k-1}^{\nu} + u_{j,k+1}^{\nu} + u_{j+1,k}^{\nu}). \tag{3.2}$$

Figure 3.2 shows that the times along lines $j+k$ are constant and that iterations in variable n occur every two time units. Hence, the proper change of variables between (3.1) and (3.2) is

$$\nu = 2n + j + k - 2. \tag{3.3}$$

The advantage of this change of variables is that the eigenmodes of (3.2) are easy to determine. They are simply Fourier modes of the form

$$u_{jk}^{\nu} = g^{\nu} \sin \xi x_j \sin \eta y_k. \tag{3.4}$$

These grid functions satisfy the boundary conditions provided that ξ and η are integer multiples of π, and substituting into (3.2) gives the following equation for g:

$$g^2 = (1-\omega) + \frac{\omega g}{2}(\cos \xi h + \cos \eta h). \tag{3.5}$$

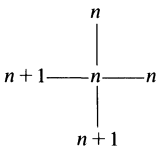

FIG. 3.1. NR *stencil in variable n.*

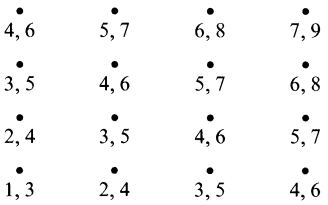

FIG. 3.2. *Times for two iterations of* NR.

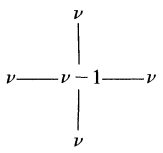

FIG. 3.3. NR *stencil in variable* ν.

For each ξ and η, this equation has two solutions, giving two eigenmodes. We obtain all modes by letting ξ and η range over the values $\xi, \eta = \pi, 2\pi, \cdots, (N-1)\pi$, for a total of $2(N-1)^2$ modes. This is the correct number since (3.2) requires two previous levels of data to calculate $u_{jk}^{\nu+1}$.

By the change of variables (3.3), an eigenvalue λ of (3.1) is g^2 and the corresponding eigenvector has components $g^{j+k} \sin \xi x_j \sin \eta y_k$. We now appear to have twice as many eigenmodes as required for (3.1), but here each mode is repeated since replacing (ξ, η) by $(N\pi - \xi, N\pi - \eta)$ simply negates the roots of (3.5). Since $\lambda = g^2$ this reflection leaves these eigenvalues unchanged. The eigenvector is also unchanged since

$$(-g)^{j+k} \sin (N\pi - \xi)x_j \sin (N\pi - \eta)y_k = g^{j+k} \sin \xi x_j \sin \eta y_k.$$

Equation (3.5) gives the famous relationship between an eigenvalue λ of SOR and an eigenvalue $\mu = \frac{1}{2}(\cos \xi h + \cos \eta h)$ of the Jacobi iteration:

$$\frac{\lambda + \omega - 1}{\omega} = \lambda^{1/2}\mu. \tag{3.6}$$

Equation (3.6) can be used to determine the optimal value of ω as a function of μ (see, e.g., Young [1971]) and this derivation will not be repeated here.

A similar analysis can be carried out for the Red/Black ordering of the grid points. In the variable n there are two stencils, one for the Red nodes and one for the Black ones, as given in Fig. 3.4. The corresponding iteration is

$$\begin{aligned} R\text{:}\quad & u_{jk}^{n+1} = (1-\omega)u_{jk}^{n} + \frac{\omega}{4}(u_{j,k+1}^{n} + u_{j,k-1}^{n} + u_{j-1,k}^{n} + u_{j+1,k}^{n}) \\ B\text{:}\quad & u_{jk}^{n+1} = (1-\omega)u_{jk}^{n} + \frac{\omega}{4}(u_{j,k+1}^{n+1} + u_{j,k-1}^{n+1} + u_{j-1,k}^{n+1} + u_{j+1,k}^{n+1}). \end{aligned} \tag{3.7}$$

The earliest times corresponding to (3.7) are given in Fig. 3.5. In the data flow variable, ν, both R and B nodes have the same stencil, namely, the stencil of Fig. 3.3. Equation (3.2) gives the update formula for all nodes. Hence, (3.5) and (3.6) also hold for the RB ordering. Figure 3.5 shows that the times along all lines with $j+k$ even are equal,

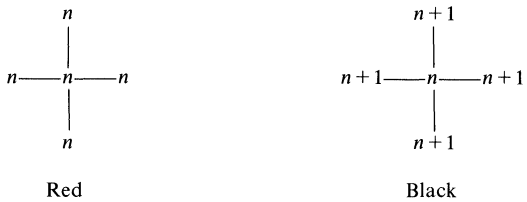

FIG. 3.4. *Red/Black stencil in variable n.*

B	*R*	*B*	*R*
2, 4	1, 3	2, 4	1, 3
R	*B*	*R*	*B*
1, 3	2, 4	1, 3	2, 4
B	*R*	*B*	*R*
2, 4	1, 3	2, 4	1, 3
R	*B*	*R*	*B*
1, 3	2, 4	1, 3	2, 4

FIG. 3.5. *Times for two iterations of RB.*

and similarly for $j+k$ odd, and that iterations in variable n occur every two time units in ν. Therefore, the change of variables is

$$\nu = 2n + [(j+k) \bmod 2] - 1,$$

and the eigenvector components of this iteration corresponding to ξ, η are

$$w_{jk} = \begin{cases} \sin \xi x_j \sin \eta y_k, \\ \lambda^{1/2} \sin \xi x_j \sin \eta y_k \end{cases}$$

for the R and B nodes, respectively. This agrees with the result given in Young [1954].

We now turn to the 9-point stencil, with orderings based on four colors. The results of Adams and Jordan [1986] applied to this model problem show that the 72 distinct four-color orderings can be grouped into six equivalence classes with regard to convergence behavior (see Fig. 3.6). Representative orderings from each of these classes are:

Ordering #1: The grid is colored as in Fig. 3.6(a) with ordering $R/B/G/O$.
Ordering #2: The grid is colored as in Fig. 3.6(b) with ordering $R/B/G/O$.
Ordering #3: The grid is colored as in Fig. 3.6(b) with ordering $R/B/O/G$.
Ordering #4: The grid is colored as in Fig. 3.6(b) with ordering $R/G/B/O$.
Ordering #5: The grid is colored as in Fig. 3.6(a) with ordering $R/B/O/G$.
Ordering #6: The grid is colored as in Fig. 3.6(a) with ordering $R/G/B/O$.

G	O	R	B
R	B	G	O
G	O	R	B
R	B	G	O

FIG. 3.6(a)

G	O	G	O
R	B	R	B
G	O	G	O
R	B	R	B

FIG. 3.6(b)

We will show that Orderings #1, #2, and #4 are in fact equivalent to the NR ordering discussed in § 2. Ordering #3 is different, however, and gives slightly slower convergence based on the spectral radius and slightly faster convergence based on the eigenvalue that dominates the iteration for smooth initial data. We have not been able to analyze either ordering #5 or ordering #6.

Ordering #1. Figure 3.7 shows the update times for this ordering, which define the data flow variable ν.

In this variable, each node has the same stencil with update formula

$$u_{jk}^{\nu+4} = (1-\omega)u_{jk}^{\nu} + \frac{\omega}{5}(u_{j-1,k}^{\nu+3} + u_{j+1,k}^{\nu+1} + u_{j,k+1}^{\nu+2} + u_{j,k-1}^{\nu+2}) + \frac{\omega}{20}(u_{j-1,k-1}^{\nu+1} + u_{j-1,k+1}^{\nu+1} + u_{j+1,k-1}^{\nu+3} + u_{j+1,k+1}^{\nu+3}). \tag{3.8}$$

G	O	R	B
3, 7	4, 8	1, 5	2, 6
R	B	G	O
1, 5	2, 6	3, 7	4, 8
G	O	R	B
3, 7	4, 8	1, 5	2, 6
R	B	G	O
1, 5	2, 6	3, 7	4, 8

FIG. 3.7. *Times for two iterations with Ordering #1.*

The change of variables is given by

$$\nu = 4n + c - 3, \tag{3.9}$$

where $c = 0, 1, 2, 3$ for the R, B, G, and O nodes of Fig. 3.7, respectively.

To see that this ordering is equivalent to the NR ordering, we only need to look at the update times for the NR ordering, shown in Fig. 3.8.

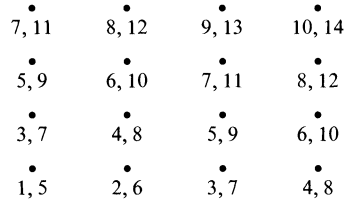

FIG. 3.8. *Times for the* 9*-point* NR *ordering.*

If we define the variable ν by these times, we again obtain iteration (3.8) with the change of variables

$$\nu = 4n + 2k + j - 6. \tag{3.10}$$

Since a change of variables gives (3.8) in either case, the eigenvalues and hence convergence behavior will be identical. If g is an eigenvalue of (3.8), then $\lambda = g^4$ is an eigenvalue of both NR and Ordering #1.

The eigenvectors, however, will not be the same, since a different change of variables is used in each case. The eigenvectors for the NR ordering were determined in § 2. Using these and the above changes of variables allows us to determine the eigenvectors for Ordering #1. In analyzing (3.8) we view it as applying to all mesh joints (j, k) at each level of ν, although in our applications it is applied only to points of a single color in each step. (Note that we could apply it to all points without affecting the results, but the work required would be increased by a factor of 4.) Since (3.8) requires four levels of prior data to determine $u_{jk}^{\nu+4}$, an eigenvector of (3.8) consists of $4(N-1)^2$ values,

$$V = \begin{bmatrix} V^0 \\ V^1 \\ V^2 \\ V^3 \end{bmatrix},$$

where $V^\nu = \{V_{jk}^\nu\}$ for $j, k = 1, 2, \cdots, N-1$. If g is the corresponding eigenvalue, then

$$\begin{bmatrix} V^1 \\ V^2 \\ V^3 \\ V^4 \end{bmatrix} = g \begin{bmatrix} V^0 \\ V^1 \\ V^2 \\ V^3 \end{bmatrix}.$$

This indicates that $V^{\nu+1} = gV^\nu$ for each ν, and hence

$$V = \begin{bmatrix} V^0 \\ gV^0 \\ g^2V^0 \\ g^3V^0 \end{bmatrix} \in R^{4(N-1)^2}.$$

If we now let V_R^0 be the vector consisting only of the values V_{jk}^0 for which (j, k) is a red point, and similarly for V_B^0, V_G^0 and V_O^0, then an eigenvector of the original iteration in the n variable (with Ordering #1) has the form

$$V^{(\#1)} = \begin{bmatrix} V_R^0 \\ gV_B^0 \\ g^2 V_G^0 \\ g^3 V_O^0 \end{bmatrix} \in R^{(N-1)^2} \tag{3.11}$$

with eigenvalue $\lambda = g^4$.

On the other hand, by the change of variables (3.10), an eigenvector for the NR ordering in the n variable has the form

$$V_{jk}^{(\mathrm{NR})} = g^{2k+j} V_{jk}^0$$

again with eigenvalue $\lambda = g^4$. Equation (2.11) gives the eigenvector for the NR ordering,

$$V_{jk}^{(\mathrm{NR})} = \alpha^k [(\Phi_1/\Phi_2)^{1/2}]^j \sin \xi x_j \sin \eta y_k,$$

where Φ_1 and Φ_2 are given by (2.7) and $\alpha = \lambda^{1/2} = g^2$. Using this we obtain

$$\begin{aligned} V_{jk}^0 &= g^{-2k-j} V_{jk}^{(\mathrm{NR})} \\ &= g^{-j} [(\Phi_1/\Phi_2)^{1/2}]^j \sin \xi x_j \sin \eta y_k. \end{aligned}$$

The eigenvectors are now determined by (3.12) with $\xi, \eta = \pi, 2\pi, \cdots, (N-1)(\pi/2)$. As before, the frequencies $\xi, \eta = ((N-1)/2+1)\pi, \cdots, (N-1)\pi$ give repeats of the eigenvalue-eigenvector pairs already found.

Ordering #2. For Ordering #2, the associated earliest times for the first two iterations are given in Fig. 3.9. An inspection of Fig. 3.9 shows that the R and G nodes have the same stencil in the variable ν, with the following update formula:

$$\begin{aligned} R, G: \quad u_{jk}^{\nu+4} &= (1-\omega) u_{jk}^{\nu} + \frac{\omega}{5} (u_{j-1,k}^{\nu+1} + u_{j+1,k}^{\nu+1} + u_{j,k-1}^{\nu+2} + u_{j,k+1}^{\nu+2}) \\ &\quad + \frac{\omega}{20} (u_{j-1,k-1}^{\nu+3} + u_{j-1,k+1}^{\nu+3} + u_{j+1,k-1}^{\nu+3} + u_{j+1,k+1}^{\nu+3}). \end{aligned} \tag{3.12}$$

Likewise, the B and O nodes have the same stencil with update formula:

$$\begin{aligned} B, O: \quad u_{jk}^{\nu+4} &= (1-\omega) u_{jk}^{\nu} + \frac{\omega}{5} (u_{j-1,k}^{\nu+3} + u_{j+1,k}^{\nu+3} + u_{j,k-1}^{\nu+2} + u_{j,k+1}^{\nu+2} \\ &\quad + \frac{\omega}{20} (u_{j-1,k-1}^{\nu+1} + u_{j-1,k+1}^{\nu+1} + u_{j+1,k-1}^{\nu+1} + u_{j+1,k+1}^{\nu+1}). \end{aligned} \tag{3.13}$$

G	*O*	*G*	*O*
3, 7	4, 8	3, 7	4, 8
R	*B*	*R*	*B*
1, 5	2, 6	1, 5	2, 6
G	*O*	*G*	*O*
3, 7	4, 8	3, 7	4, 8
R	*B*	*R*	*B*
1, 5	2, 6	1, 5	2, 6

FIG. 3.9. *R/B/G/O times for Ordering #2.*

The change of variables from n to ν is again given by (3.9), where $c=0, 1, 2$ and 3 for the R, B, G and O equations, respectively.

Now, the equations in (3.12) and (3.13) have the symmetry needed to verify that $V^0_{jk}=\sin \xi x_j \sin \eta y_k$. Thus the methods in (3.12) and (3.13) have the same value for V^0_{jk} but different amplification factors, say g_1 and g_2. A single step of the full method, in variable n, consists of four sweeps, two with (3.12) and two with (3.13) and hence has amplification factor

$$\lambda = g_1^2 g_2^2.$$

In order to determine λ, we find $\alpha = g_1 g_2$ by considering two sweeps of the method, Red and Black, say. We substitute the following values

$$\begin{aligned} u^{\nu}_{jk} &= e^{i(\xi x_j + \eta y_k)}, \\ u^{\nu+1}_{jk} &= g_2 u^{\nu}_{jk}, \\ u^{\nu+2}_{jk} &= g_1 g_2 u^{\nu}_{jk}, \\ u^{\nu+3}_{jk} &= g_1 g_2^2 u^{\nu}_{jk}, \\ u^{\nu+4}_{jk} &= g_1^2 g_2^2 u^{\nu}_{jk}, \\ u^{\nu+5}_{jk} &= g_1^2 g_2^3 u^{\nu}_{jk}, \end{aligned} \tag{3.14}$$

into (3.12) to get

$$g_1^2 g_2^2 = (1-\omega) + \frac{\omega}{5}(2g_2 \cos \xi h + 2g_1 g_2 \cos \eta h + g_1 g_2^2 \cos \xi h \cos \eta h). \tag{3.15}$$

Next, we take a step with (3.13) to update the Black nodes, and obtain $u^{\nu+5}_{jk}$. Putting (3.14) into (3.13) for $\nu+5$ we get

$$g_1^2 g_2^2 = (1-\omega) + \frac{\omega}{5}(2g_1^2 g_2 \cos \xi h + 2g_1 g_2 \cos \eta h + g_1 \cos \xi h \cos \eta h). \tag{3.16}$$

Equations (3.15) and (3.16) can be equated and g_1 and g_2 eliminated to give a quartic equation for α. Surprisingly, this quartic is again (2.10), the quartic obtained in our analysis of the NR ordering by separation of variables. This shows that this ordering is equivalent to the NR ordering, and hence is also equivalent to Ordering #1.

The eigenvectors in the variable n can be seen from (3.9) and (3.14) to be

$$V^{(\#2)} = \begin{bmatrix} V^0_R \\ g_2 V^0_B \\ g_1 g_2 V^0_G \\ g_1 g_2^2 V^0_O \end{bmatrix} \in R^{(N-1)^2}$$

where $V^0_{jk}=\sin \xi x_j \sin \eta y_k$, $\xi, \eta = \pi, 2\pi, \cdots, (N-1)(\pi/2)$ with eigenvalue $\lambda = g_1^2 g_2^2$. Again, we find that eigenvalue-eigenvector pairs are repeated for the frequencies $((N-1)/2+1)\pi, \cdots, (N-1)\pi$.

Ordering #3. For this ordering, the earliest times for the first two iterations are given in Fig. 3.10. The R and O nodes have the same stencil in the variable ν with the following update formula:

$$\begin{aligned} R, O: \quad u^{\nu+4}_{jk} = (1-\omega)u^{\nu}_{jk} &+ \frac{\omega}{5}(u^{\nu+3}_{j,k+1} + u^{\nu+3}_{j,k-1} + u^{\nu+1}_{j+1,k} + u^{\nu+1}_{j-1,k}) \\ &+ \frac{\omega}{20}(u^{\nu+2}_{j-1,k-1} + u^{\nu+2}_{j-1,k+1} + u^{\nu+2}_{j+1,k-1} + u^{\nu+2}_{j+1,k+1}). \end{aligned} \tag{3.17}$$

G	*O*	*G*	*O*
4, 8	3, 7	4, 8	3, 7
R	*B*	*R*	*B*
1, 5	2, 6	1, 5	2, 6
G	*O*	*G*	*O*
4, 8	3, 7	4, 8	3, 7
R	*B*	*R*	*B*
1, 5	2, 6	1, 5	2, 6

FIG. 3.10. *R/B/O/G times for Ordering #3.*

Likewise, the B and G nodes are updated by the formula

$$B, G: \quad u_{jk}^{\nu+4} = (1-\omega)u_{jk}^{\nu} + \frac{\omega}{5}(u_{j,k+1}^{\nu+1} + u_{j,k-1}^{\nu+1} + u_{j+1,k}^{\nu+3} + u_{j-1,k}^{\nu+3}) + \frac{\omega}{20}(u_{j-1,k-1}^{\nu+2} + u_{j-1,k+1}^{\nu+2} + u_{j+1,k-1}^{\nu+2} + u_{j+1,k+1}^{\nu+2}). \tag{3.18}$$

Substituting (3.14) into (3.17) and (3.18) yields

$$g_1^2 g_2^2 = (1-\omega) + \frac{2\omega}{5}(g_1 g_2^2 \cos \eta h + g_2 \cos \xi h) + \frac{\omega}{5} g_1 g_2 \cos \eta h \cos \xi h \tag{3.19}$$

and

$$g_1^2 g_2^2 = (1-\omega) + \frac{2\omega}{5}(g_1 \cos \eta h + g_1^2 g_2 \cos \xi h) + \frac{\omega}{5} g_1 g_2 \cos \xi h \cos \eta h, \tag{3.20}$$

respectively. As before, we equate (3.19) and (3.20), eliminate g_1 and g_2, and get the following quartic in $\alpha = g_1 g_2$:

$$\begin{aligned} &\alpha^4 - (\tfrac{2}{5}\omega \cos \eta h \cos \xi h + \tfrac{4}{25}\omega^2 \cos \eta h \cos \xi h)\alpha^3 \\ &+ (\tfrac{1}{25}\omega^2 \cos^2 \eta h \cos^2 \xi h + 2(\omega - 1) - \tfrac{4}{25}\omega^2 \cos^2 \eta h - \tfrac{4}{25}\omega^2 \cos^2 \xi h)\alpha^2 \\ &+ (\tfrac{2}{5}\omega(1-\omega) \cos \eta h \cos \xi h - \tfrac{4}{25}\omega^2 \cos \xi h \cos \eta h)\alpha + (\omega - 1)^2 = 0. \end{aligned} \tag{3.21}$$

The change of variables from n to ν is again given by (3.9) where $c = 0, 1, 2$, and 3 correspond to the R, B, O, and G equations, respectively. Following the same arguments as before, we find that the eigenvectors in variable n for Ordering #3 are given by

$$V^{(\#3)} = \begin{bmatrix} V_R^0 \\ g_2 V_B^0 \\ g_1 g_2^2 V_G^0 \\ g_1 g_2 V_O^0 \end{bmatrix} \in R^{(N-1)^2},$$

where $V_{jk}^0 = \sin \xi x_j \sin \eta y_k$, $\xi, \eta = \pi, 2\pi, \cdots, (N-1)(\pi/2)$ and the eigenvalue is $\lambda = g_1^2 g_2^2$. Again, we find that eigenvalue-eigenvector pairs are repeated for $\xi, \eta = ((N-1)/2+1)\pi, \cdots, (N-1)\pi$. This can be seen for the eigenvalues from (3.21) since replacing (ξ, η) by $(N\pi - \xi, N\pi - \eta)$ leaves the quartic unchanged and replacing (ξ, η) by either $(N\pi - \xi, \eta)$ or $(\xi, N\pi - \eta)$ negates the coefficient of the α and α^3 terms.

The quartic in (3.21) does not agree with the quartic in (2.10), and the roots do not agree in general. Consequently, the optimal ω and corresponding convergence rate are different for this ordering than for the other orderings considered so far.

Numerical results show that the roots of (3.21) have the same qualitative behavior as shown in Fig. 2.1 with $\xi = \eta = \pi$ giving the slowest decay. The optimal ω is also seen to occur where the largest real root and the complex root of largest modulus intersect for the frequencies $\xi = \eta = \pi$. We confirm these observations by performing an identical analysis to that given in § 2 for the rowwise ordering. We summarize our results below.

The complex root of (3.21) with largest modulus for small h occurs when $\xi = \eta = \pi$ and is

$$e^{i\theta_1}(1 - \tfrac{3}{8}k_1 h) + O(h^2) \tag{3.22}$$

where $\theta_1 = \cos^{-1}(-\frac{7}{25})$.

The largest real root of (3.21) for small h also occurs when $\xi = \eta = \pi$ and is

$$1 - c_1 h + O(h^2) \tag{3.23}$$

where

$$c_1 = \tfrac{5}{8}k_1 - \tfrac{1}{8}\sqrt{25k_1^2 - 96\pi^2}. \tag{3.24}$$

The optimal ω occurs when the modulus of the root in (3.22) equals the modulus of the root in (3.23). This value of ω is

$$\omega_{\text{opt}} = 2 - \frac{4\sqrt{6}}{\sqrt{21}}\pi h + O(h^2) \approx 2 - 2.138\pi h. \tag{3.25}$$

The corresponding value of the spectral radius is

$$\rho_{\text{opt}} = 1 - 2c_1 h + O(h^2) \approx 1 - 1.604\pi h. \tag{3.26}$$

This RBOG SOR iteration was programmed and the results of (3.25) and (3.26) confirmed. By comparing (2.25) and (3.26), we see that different evaluation orderings for the same coloring of the grid points can lead to different asymptotic convergence rates, based on the spectral radius.

The eigenvector associated with the spectral radius is highly oscillatory as the mesh is refined (recall that this was true for the rowwise ordering also). An analysis similar to Garabedian's can be performed to find the convergence behavior for smooth initial data. To do this, we choose k_1 to maximize c_1 in (3.24) to get

$$k_1 = \tfrac{4}{5}\sqrt{6}\pi \approx 1.95959\pi$$

and

$$2c_1 = \sqrt{6}\pi \approx 2.44949\pi.$$

The corresponding values of ρ^*_{opt} and ω^*_{opt} are

$$\rho^*_{\text{opt}} = 1 - 2.44949\pi h, \qquad \omega^*_{\text{opt}} = 2 - 1.95959\pi h. \tag{3.27}$$

The values in (3.27) show that for smooth initial data this ordering is preferred over the rowwise ordering and Orderings #1 and #2. Note that the values in (3.25) and (3.26), based on the true spectral radius, lead to the opposite conclusion. However, the results of (3.25) and (3.26) are valid for nonsmooth initial data. Figure 3.11 shows the decay of $\|u\|_2$ for various initial data. For initial data obtained by discretizing the smooth data $u(x, y) = (x^2 - x)(y^2 - y)$, the observed decay is initially much closer to that predicted by (3.27), than to ρ^n.

Ordering #4. This ordering leads to a quartic equivalent to (2.10) with ξ and η interchanged. Hence, for a square grid with stepsize h in both the x and y directions, ω_{opt} and ρ_{opt} for this ordering are also given by (2.25).

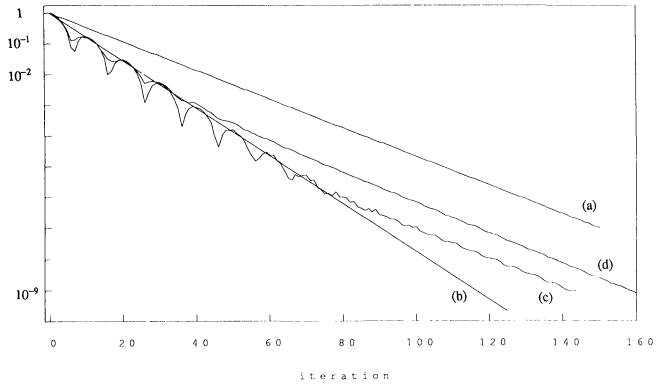

FIG. 3.11. *Convergence history* (2*-norm of error versus iteration number*) *for Ordering* #3 *with* $h = 0.05$ *and* $\omega = 1.86$. *Three choices of initial data are compared*: (a) *An eigenvector corresponding to the spectral radius.* (b) *An eigenvector corresponding to the largest nonspurious eigenvalue.* (c) $u^0_{jk} = (x_j^2 - x_j)(y_k^2 - y_k)$. (d) $u^0_{jk} = 1$.

Any of the twenty-four possible orderings associated with Fig. 3.6(b) can be easily proved to have the same eigenvalues as Ordering #2 or Ordering #3 that we have analyzed here (Adams and Jordan [1986]). We have found two equivalence classes that characterize the asymptotic convergence rate behavior and the relaxation parameter ω. Orderings #1, #2, and #4 belong to the first class and Ordering #3 belongs to the second one. In addition, there could be two more classes corresponding to Orderings #5 and #6 that we have not been able to analyze.

4. A 9-point pseudo-SOR method. We now consider a pseudo-SOR method with the stencil in Fig. 4.1, and iteration

$$u^{n+1}_{jk} = (1-\omega)u^n_{jk} + \frac{\omega}{5}(u^{n+1}_{j,k-1} + u^{n+1}_{j-1,k} + u^n_{j+1,k} + u^n_{j,k+1}) + \frac{\omega}{20}(u^n_{j-1,k+1} + u^{n+1}_{j-1,k-1} + u^{n-1}_{j+1,k+1} + u^n_{j+1,k-1}) \tag{4.1}$$

which differs from (2.1) in the last two terms. This method can be analyzed by the techniques of § 3. The earliest times for two iterations corresponding to Fig. 4.1 are equal to those of Fig. 3.2. That is, the iteration expressed in terms of the variable ν is

$$u^{\nu+1}_{jk} = (1-\omega)u^{\nu-1}_{jk} + \frac{\omega}{5}(u^{\nu}_{j,k-1} + u^{\nu}_{j-1,k} + u^{\nu}_{j+1,k} + u^{\nu}_{j,k+1}) + \frac{\omega}{20}(u^{\nu-1}_{j-1,k+1} + u^{\nu-1}_{j-1,k-1} + u^{\nu-1}_{j+1,k+1} + u^{\nu-1}_{j+1,k-1}), \tag{4.2}$$

with the change of variables given by (3.3). It is interesting to note that the times in Fig. 3.5 and the iteration in (4.2) are also obtained for an RB ordering of the grid with

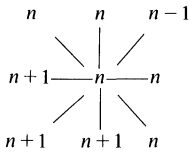

FIG. 4.1. NR *modified stencil in variable n.*

the Red and Black stencils shown in Fig. 4.2. Since two colors do not decouple a grid discretized with the 9-point stencil, it is tempting to use old information for the Black to Black coupling as shown in Fig. 4.2 to obtain a method suitable for parallel computers. This modification was considered by Kuo, Levy, and Musicus [1986] for a 9-point stencil arising from a discretization of a PDE with a cross-derivative term. They show the convergence rate of SOR for their problem to be $1-O(h)$ in the region where the lowest frequency dominates. We show by analyzing (4.2) that the use of only two colors is not sufficient for the 9-point stencil arising from the Laplacian. In particular, we will show that the method converges whenever $0<\omega<\frac{5}{3}$, that the optimal ω occurs where the lowest and highest frequencies cross, and that the rate of convergence with the optimal ω is approximately $1-3\pi^2h^2$ for small h as opposed to the result $1-1.79\pi h$ obtained in § 3 for the true SOR method with Orderings #1 or #2.

We begin by observing that $u_{jk}^{\nu}=g^{\nu}\sin \xi x_j \sin \eta y_k$ is an eigenmode of (4.2). We substitute this into (4.2) to get

$$g^2=(1-\omega)+\frac{2g\omega}{5}(\cos \xi h+\cos \eta h)+\frac{\omega}{5}\cos \xi h \cos \eta h, \tag{4.3}$$

where g^2 is the eigenvalue of the method in (4.1) or the RB method depicted in Fig. 4.2. The eigenvectors in variable n for the NR ordering (4.1) or the RB ordering (Fig. 4.2) are the same as the respective ones given in § 3 for the 5-point stencil.

Equation (4.3) can be solved for g to get

$$g=\frac{\omega}{5}(\cos \xi h+\cos \eta h)\pm\sqrt{\frac{\omega^2}{25}(\cos \xi h+\cos \eta h)^2+(1-\omega)+\frac{\omega}{5}\cos \xi h \cos \eta h}. \tag{4.4}$$

When $\omega=1$, the "pseudo Gauss-Seidel" method has amplification factor

$$g_{\pm}^2=\left(\frac{\cos \xi h+\cos \eta h}{5}\pm\sqrt{\frac{1}{25}(\cos \xi h+\cos \eta h)^2+\frac{1}{5}(\cos \xi h \cos \eta h)}\right)^2, \tag{4.5}$$

which is maximized when $\xi=\eta=\pi$. The maximum value is easily determined from (4.5) to be $\cos^2 \pi h$. This is identical to the spectral radius of Gauss-Siedel for the model problem with the 5-point stencil. The methods, however, differ drastically when $\omega\neq 1$.

To determine the optimal ω, we must minimize the maximum modulus of g in (4.4). Two cases must be considered. First, assume the radical in (4.4) is negative. Then

$$|g|^2=\omega(1-\tfrac{1}{5}\cos \xi h \cos \eta h)-1, \tag{4.6}$$

and for convergence, we require $|g|^2<1$, and hence

$$0<\omega<\frac{2}{1-\frac{1}{5}\cos \xi h \cos \eta h}. \tag{4.7}$$

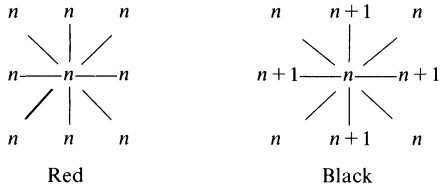

FIG. 4.2. RB 9-*point modified stencil in variable n.*

As $h \to 0$, (4.7) shows that the method is divergent for $\omega > \frac{5}{3}$. Also (4.6) shows that the value of $|g|^2$ is maximized when $\cos \xi h = -\cos \eta h$. This occurs when $\eta = N - \xi$ (low frequency in one direction and high frequency in the other) and this maximum is

$$|g|^2_{\max} = \omega(1 + \tfrac{1}{5}\cos^2 \pi h) - 1. \tag{4.8}$$

As $h \to 0$, $|g|^2_{\max} \to |\frac{6}{5}\omega - 1|$.

Second, assume the radical in (4.4) is positive. Then, the maximum value of g occurs when $\xi = \eta = \pi$ and is

$$\begin{aligned} g^2_{\max} = {} & \frac{8}{25}\omega^2 \cos^2 \pi h + (1-\omega) + \frac{\omega}{5}\cos^2 \pi h \\ & + \frac{4}{5}\omega \cos \pi h \sqrt{\frac{4}{25}\omega^2 \cos^2 \pi h + (1-\omega) + \frac{\omega}{5}\cos^2 \pi h}. \end{aligned} \tag{4.9}$$

It is interesting to note that the ω that minimizes (4.9) occurs when the radical is zero, and as $h \to 0$, $\omega \to 5/2$. That is, the method is divergent for the ω that minimizes $g^2_{\max}$ of (4.9) for the lowest frequency. Recall that the ω that is optimal for SOR for consistently ordered matrices corresponds to the lowest frequency. For the pseudo-SOR method, the optimal ω occurs where the modulus of the eigenvalues of the two frequencies $\eta = N - \xi$ and $\eta = \xi = \pi$ are equal. This ω is determined by equating (4.8) and (4.9) to get

$$\frac{16\omega^2 \cos^2 \pi h}{25}\left(\frac{\omega}{5}\cos^2 \pi h + \omega - 1\right) - 4(\omega - 1)^2 = 0. \tag{4.10}$$

As $h \to 0$, $\omega \to 5/3$, so we look for a solution to (4.10) of the form

$$\omega(h) = \tfrac{5}{3} + c_1 h + c_2 h^2 + \cdots. \tag{4.11}$$

Substituting (4.11) into (4.10) and equating terms yields

$$c_1 = 0, \qquad c_2 = -\tfrac{20}{9}\pi^2,$$

and the corresponding values of the optimal ω and spectral radius of (4.1) are

$$\omega_{\text{opt}} \approx \tfrac{5}{3} - \tfrac{20}{9}\pi^2 h^2, \qquad \rho_{\text{opt}} \approx 1 - 3\pi^2 h^2. \tag{4.12}$$

Comparing (4.12) to $\cos^2 \pi h \approx 1 - \pi^2 h^2$, the spectral radius of the pseudo-Gauss-Seidel method, shows that as $h \to 0$, this method with optimal ω is only three times faster than with $\omega = 1$. This is not nearly as good as the true SOR methods discussed in § 3, where the decay factor is $1 - O(h)$ for the optimal ω.

5. Comparison of point and line methods. Let the system $Ax = b$ be blocked as

$$\begin{bmatrix} D_1 & -U_{12} & \cdots & -U_{1m} \\ -L_{21} & D_2 & \cdots & -U_{2m} \\ \vdots & -L_{32} & \cdots & \vdots \\ \vdots & \vdots & \cdots & \\ -L_{m1} & -L_{m2} & \cdots & D_m \end{bmatrix} \begin{bmatrix} u_1 \\ u_2 \\ \vdots \\ \vdots \\ u_m \end{bmatrix} = \begin{bmatrix} b_1 \\ b_2 \\ \vdots \\ \vdots \\ b_m \end{bmatrix}.$$

The line-Jacobi method is defined as

$$D_i u_i^{n+1} = \sum_{j<i} L_{ij} u_j^n + \sum_{j>i} U_{ij} u_j^n + b_i \tag{5.1}$$

and the line-SOR method as

$$D_i u_i^{n+1} = \omega \sum_{j<i} L_{ij} u_j^{n+1} + \omega \sum_{j>i} U_{ij} u_j^n + \omega b_i + (1-\omega) D_i u_i^n,$$

where for both methods u_i corresponds to the nodes in row i of the grid. The spectral radius of the Jacobi method for the 5-point and 9-point stencils can easily be found by separation of variables, since $\sin \xi x_j \sin \eta y_k$ is an eigenvector of iteration (5.1). These results are given in Fig. 5.1.

The spectral radius of the line-SOR method for the 5-point and 9-point stencils can now be found using Young's theory for block-consistently ordered matrices. That is, if μ is the spectral radius of line-Jacobi, then ω_{opt} and $\rho_{\text{opt}}$for line-SOR are given by

$$\omega_{\text{opt}} = \frac{2}{1+\sqrt{1-\mu^2}}, \qquad \rho_{\text{opt}} = \omega_{\text{opt}} - 1. \tag{5.2}$$

These SOR results are summarized in Fig. 5.2, where Garabedian's results for the 9-point point methods are given in parentheses. Figure 5.2 shows that, based on the actual spectral radius, the line methods converge faster than the point methods for both the 5 and 9 point stencils. The 9-point line SOR method has the same convergence rate as the 5-point line SOR method for small h; whereas the 5-point SOR method with a consistent ordering can be expected to converge slightly faster than any of the 9-point point SOR methods that we analyzed. However, the convergence rate will be observed in practice with smooth initial data for the 9-point point methods may be closer to Garabedian's results. That is, we can still expect the 9-point line methods to converge slightly faster than the point methods, but now, the 9-point point methods will converge faster than the 5-point point method. This latter fact is encouraging since the 9-point discretization is more accurate than the 5-point one.

Method	Spectral radius
5-point point	$\cos \pi h \approx 1 - \frac{1}{2}\pi^2 h^2$
5-point line	$\dfrac{\cos \pi h}{2 - \cos \pi h} \approx 1 - \pi^2 h^2$
9-point point	$\frac{4}{5}\cos \pi h + \frac{1}{5}\cos^2 \pi h \approx 1 - \frac{3}{5}\pi^2 h^2$
9-point line	$\dfrac{\frac{2}{5}\cos \pi h + \frac{1}{5}\cos^2 \pi h}{1 - \frac{2}{5}\cos \pi h} \approx 1 - \pi^2 h^2$

FIG. 5.1. *Spectral radius of point and line Jacobi methods.*

Method	Ordering	Spectral radius ρ_{opt} (ρ^*_{opt})
5-point point	Rowwise or Red/Black	$1 - 2\pi h$
5-point line	Rowwise or Red/Black	$1 - 2\sqrt{2}\pi h$
9-point point	Ordering #1	$1 - 1.79\pi h$ $(1 - 2.35\pi h)$
9-point point	Ordering #2	$1 - 1.79\pi h$ $(1 - 2.35\pi h)$
9-point point	Ordering #3	$1 - 1.60\pi h$ $(1 - 2.45\pi h)$
9-point point	Rowwise	$1 - 1.79\pi h$ $(1 - 2.35\pi h)$
9-point line	Rowwise or Red/Black	$1 - 2\sqrt{2}\pi h$

FIG. 5.2. *Spectral radius for point and line* SOR *methods.*

6. Conclusions. The SOR method with several orderings and a pseudo-SOR method have been analyzed for the 9-point Laplacian. The Fourier analysis techniques proposed by LeVeque and Trefethen [1986] and separation of variables techniques were used to determine the eigenvalues and the eigenvectors of these methods.

We examined the SOR method for the 9-point Laplacian using the natural rowwise ordering and several multicolor orderings. For all these orderings, we gave a quartic equation for the square root of the eigenvalues as a function of the frequencies and ω. The optimal ω was found for the rowwise ordering and Ordering #3 by asymptotically solving a quartic equation for the intersection of the largest (in modulus) of the complex and real roots.

Our results were confirmed by performing the SOR iteration with an initial guess corresponding to the eigenvector associated with the spectral radius. The observed rate of convergence matched that predicted by the theory to five decimal places. The SOR iteration was also performed by using a smooth initial guess, obtained by discretizing $(x-x^2)(y-y^2)$ for various stepsizes, h. In these cases, the observed convergence rate more closely resembled that predicted by Garabedian.

The results also show that different orderings of the same coloring can lead to different spectral radii: $R/B/G/O$ and $R/B/O/G$ for the coloring in Fig. 3.6(b) have spectral radii of $1-1.79\pi h$ and $1-1.60\pi h$, respectively. For smooth initial data, these two orderings also led to different effective spectral radii observed in practice, namely, $1-2.35\pi h$ and $1-2.45\pi h$, respectively. This information can be useful in selecting a coloring, an ordering, and appropriate initial data to use with multicolor SOR on parallel computers (Adams and Ortega [1982]).

An analysis of the pseudo-SOR method showed that the optimal ω occurs when the high and low frequencies cross and that the corresponding spectral radius is only $1-3\pi^2h^2$. This is inferior to both the 5-point and 9-point SOR methods we analyzed. In addition, for small h, the pseudomethod only converges for $0<\omega<\frac{5}{3}$.

The 5-point and 9-point and line SOR methods were compared for the model problem for small h. The line methods converge slightly faster than the point methods. The 9-point line and 5-point line methods have the same asymptotic rate of convergence, but the 5-point point method with a consistent ordering was 1.12 times faster, based on the spectral radius, and 1.23 times slower, based on Garabedian's arguments, than the best 9-point point method that we analyzed. Hence, for a smooth initial guess, the 9-point point methods can be expected to be more accurate and converge faster than the 5-point point method.

Acknowledgments. The authors thank Lloyd N. Trefethen for providing the initial stimulus for this work and for several valuable subsequent conversations. We also thank Elizabeth Ong for programming the SOR method with our orderings.

Note added in proof. In unpublished work carried out in 1951, the third listed author of this paper used the method of separation of variables to derive the quartic equation (2.13) for the eigenvalues of the SOR method for the 9-point equation with the rowwise ordering. Because of the lack of sufficient computational faculties, he was unable to use this equation to determine the optimum value of ω and the corresponding convergence rate of the SOR method. The work lay dormant until its resurrection in the summer of 1986.

Richard Varga and John Buoni brought to our attention that an analysis of the SOR method for the 9-point equation with the rowwise ordering had been carried out

by A. I. van de Vooren and A. C. Vliegenthart [1967]. This analysis includes cases where the mesh sizes Δx and Δy in the x and y directions, respectively, may be different. For the case where $\Delta x = \Delta y$, the authors obtain the same asymptotic results for the spectral radius as given by (2.25). In this section, we have carried these results further by finding the eigenvectors as well. These eigenvectors were used in our numerical experiments as starting data to verify (2.25). The eigenvectors were also used to explain the discrepancy between Garabedian's results and those given in (2.25).

REFERENCES

L. M. ADAMS AND J. M. ORTEGA [1982], *A multi-color* SOR *method for parallel computation*, Proc. of the 1982 Conference on Parallel Processing, IEEE Catalog N. 82CH1794-7, August, pp. 53–56.

L. M. ADAMS AND H. F. JORDAN [1986], *Is* SOR *Color-blind?*, SIAM J. Sci. Statist. Comput., 7, pp. 490–506.

G. FORSYTHE AND W. WASOW [1960], *Finite-Difference Methods for Partial Differential Equations*, John Wiley, New York, p. 266.

S. FRANKEL [1950], *Convergence rates of iterative treatments of partial differential equations*, Math. Comp., 4, pp. 65–75.

P. GARABEDIAN [1956], *Estimation of the relaxation factor for small mesh size*, Math. Comp., 10, pp. 183–185.

C. KUO, B. LEVY, AND B. MUSICUS [1986], *A local relaxation method for solving elliptic* PDE*s on mesh-connected arrays*, SIAM J. Sci. Statist. Comput., accepted.

R. LEVEQUE AND L. N. TREFETHEN [1986], *Fourier analysis of the* SOR *iteration*, ICASE Report No. 86-93, ICASE-NASA Langley Research Center, Hampton, VA, to appear in IMA J. Num. Anal.

A. I. VAN DE VOOREN AND A. C. VLIEGENTHART [1967], *The 9-point difference formula for Laplace's equation*, J. Engr. Math., 1, pp.187–202.

D. M. YOUNG [1954], *Iterative methods for solving partial differential equations of elliptic type*, Trans. Amer. Math. Soc., 76, pp. 92–111.

——— [1971], *Iterative Solution of Large Linear Systems*, Academic Press, New York.